

# Shapiro Steps and Nonlinear Skyrmion Hall Angles For dc and ac Driven Skyrmions on a Two Dimensional Periodic Substrate

N. P. Vizarim<sup>1,2</sup>, C. Reichhardt<sup>1</sup>, P. A. Venegas<sup>3</sup>, and C. J. O. Reichhardt<sup>1</sup>

<sup>1</sup>*Theoretical Division and Center for Nonlinear Studies,*

*Los Alamos National Laboratory, Los Alamos, New Mexico 87545, USA*

<sup>2</sup> *POSMAT - Programa de Pós-Graduação em Ciência e Tecnologia de Materiais, Faculdade de Ciências, Universidade Estadual Paulista - UNESP, Bauru, SP, CP 473, 17033-360, Brazil and*

<sup>3</sup> *Departamento de Física, Faculdade de Ciências, Universidade Estadual Paulista - UNESP, Bauru, SP, CP 473, 17033-360, Brazil*

(Dated: March 11, 2020)

For an overdamped particle moving over a two-dimensional periodic substrate under combined dc and ac drives, a series of steps can appear in the velocity force curves that are known as Shapiro steps. Here we show that for skyrmions driven over a two-dimensional periodic obstacle array with a dc drive and an ac drive that is either parallel or perpendicular to the dc drive, the system exhibits numerous transverse and longitudinal synchronization dynamics due to the Magnus force. These phenomena originate in interactions between two different types of phase locking effects: Shapiro steps and directional locking. In some cases, the skyrmion Hall angle is constant but longitudinal Shapiro steps appear, while in other regimes the skyrmion Hall angle can either increase or decrease with increasing dc drive during the phase locking as the skyrmion locks to different symmetry directions of the obstacle lattice. For a transverse ac drive we find that strong Hall angle overshoots can occur in certain locked phases where the skyrmion is moving at an angle that is considerably larger than the intrinsic Hall angle. For the strongest Magnus force, the phase locking effects are reduced and there are larger regions of disordered dynamics. We show that the skyrmion Hall angle can be controlled by fixing the dc drive and changing the amplitude of the ac drive.

## I. INTRODUCTION

Systems with multiple interacting frequencies are known to exhibit various nonlinear dynamical effects such as synchronization or phase locking<sup>1,2</sup>. Such phenomena arise across a wide range of fields ranging from coupled pendula<sup>3</sup> to biological systems<sup>4</sup>. One of the simplest examples of a system that can exhibit phase locking is an overdamped particle on a periodic substrate under a combined dc and ac drive, where there can be resonances between the ac driving frequency and the frequency of the oscillations generated by the motion of the particle over the periodic substrate. These resonance effects create a series of steps in the velocity force curves since the particle remains locked to a specific velocity over an interval of the external drive in order to remain in the resonant state. One of the first systems where such resonant steps were observed was Josephson junctions, where so-called Shapiro steps appear in the current-voltage response<sup>5,6</sup>. Many systems that exhibit phase locking can be described as effectively one dimensional, and locking dynamics have been studied for Josephson junction arrays<sup>7</sup>, incommensurate sliding charge density waves<sup>8,9</sup>, vortices in type-II superconductors with one-dimensional (1D)<sup>10–12</sup> and two-dimensional (2D) periodic substrates<sup>13,14</sup>, driven Frenkel-Kontorova models<sup>15</sup>, frictional systems<sup>16</sup>, and colloids moving over 1D periodic substrates<sup>17–19</sup>. Even in the 1D case, a variety of additional phenomena such as fractional locking can arise when additional nonlinear effects come into play.

Particles moving over a periodic 2D substrate exhibit

many of the same phase locking effects as the 1D systems, but the additional degrees of freedom available in 2D make it possible to align the ac drive perpendicular to the dc drive. In this case, new phase locking effects that are distinct from Shapiro steps can appear that are known as transverse phase locking, in which the step widths generally grow with increasing ac amplitude<sup>20,21</sup> rather than oscillating with increasing ac amplitude as in Shapiro steps. For 2D substrates it is also possible to have bi-harmonic ac drives applied both parallel and perpendicular to the dc drive, which generate a circular motion of the driven particle. Here, an increasing dc drive produces chiral scattering effects that result in phase locked regions in which the particle motion is both transverse and longitudinal to the dc drive direction<sup>22,23</sup>.

In most of the above systems the dynamics is overdamped; however, in some situations non-dissipative effects such as inertia can arise<sup>24</sup>. Another type of non-dissipative effect is a gyro-coupling or Magnus force, which creates velocity components that are perpendicular to the forces experienced by the particle. In a 1D system, a Magnus force has no effect; however, in 2D systems it can strongly modify the dynamics. Magnus forces can be significant or even dominating for skyrmions in chiral magnets<sup>25–28</sup>, where the ratio of the Magnus force to the damping term can vary from 0.1 to 10. Skyrmions can interact with pinning sites, be set into motion readily with an applied current, and exhibit depinning thresholds<sup>27,29–34</sup>. One of the most prominent effects of the Magnus force is that the skyrmions move at an angle with respect to the applied driving force which is known as the skyrmion Hall angle  $\theta_{sk}$ <sup>27</sup>, as has

been observed in simulations<sup>35–38</sup> and experiments<sup>39,40</sup>. The Magnus force strongly modifies the interaction of the skyrmion with a substrate by creating spiraling motions of skyrmions that are in a trapping potential<sup>40–46</sup>. The pinning or defects produce a strong drive dependence of the skyrmion Hall angle, which starts off near zero just at depinning and increases with increasing skyrmion velocity before saturating to the intrinsic value at high drives. This effect was first observed in simulations of skyrmions interacting with periodic or random disorder<sup>36–38,42,47,48</sup> and was then found in experiments<sup>39,40,49–52</sup>. The drive dependence arises due to a side jump effect when the skyrmion scatters off a pinning site<sup>36,42</sup>. For random disorder,  $\theta_{sk}$  increases smoothly with increasing drive; however, for a periodic substrate a guiding effect occurs which causes the skyrmion motion to become directionally locked to specific symmetry directions of the substrate over a range of drives, producing a quantized skyrmion Hall angle<sup>36,53</sup>. There are a number of proposals on how to create localized skyrmion pinning sites, which can be attractive or repulsive<sup>54–57</sup>, and there are now experimental realizations of skyrmion phases in periodic substrates<sup>58</sup> and superconducting vortices interacting with skyrmions<sup>59</sup>, making it feasible to create tailored 2D pinning arrays of attractive or repulsive obstacles with which skyrmions can interact.

Skyrmions moving over a 2D substrate under dc and ac drives are expected to exhibit a variety of new synchronization effects not observed in overdamped systems. In numerical work examining dc and ac driven skyrmions in 2D systems moving over a periodic 1D substrate, Shapiro steps appeared for the velocity in both the longitudinal and transverse directions<sup>60</sup>. In an overdamped 2D system with a 1D substrate, phase locking occurs only when the dc drive, ac drive, and substrate periodicity direction are all aligned. The inclusion of the Magnus force allows any combination of the ac and dc drive directions to produce some form of phase locking, and also generates new effects such as Shapiro spikes in the velocity force curves, which are distinct from Shapiro steps<sup>61</sup>. It is even possible for absolute transverse mobility to appear in which the skyrmion moves at  $90^\circ$  to the driving direction, as well as negative mobility in which the net skyrmion motion is in the direction opposite to the applied drive<sup>61</sup>, or ratchet effects<sup>62,63</sup>. The Magnus force opens entirely new aspects of nonlinear dynamics, and skyrmions moving over periodic substrates can serve to provide experimental realizations of such dynamics. These results suggest that skyrmion motion can be controlled by combining a periodic substrate array with different driving protocols, which can be important for applications<sup>64</sup>.

In this work we extend our previous results on dc and ac driven skyrmions on a 1D periodic array<sup>60,61,65</sup> to the case of skyrmions interacting with a 2D periodic array of obstacles, where the ac drive can be applied either parallel or perpendicular to the dc drive direction. We find two dominant effects. The first is directional locking, which is similar to that found previously for purely

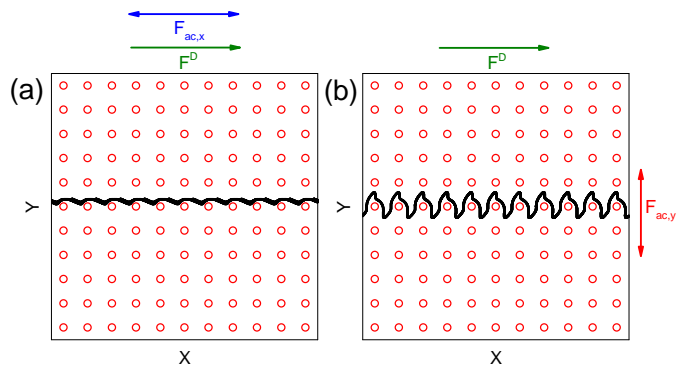


FIG. 1. A schematic of the system, which consists of a square array of obstacles (red circles) modeled as repulsive Gaussian scattering sites. The black line is the trajectory of a skyrmion which is subjected to both damping and a Magnus term as well as a dc drive  $F^D$  applied along the  $x$  direction. An additional ac drive is applied either (a) along the  $x$  direction,  $F_{ac,x}$ , or (b) along the  $y$  direction,  $F_{ac,y}$ .

dc driven skyrmions on a 2D substrate<sup>37,53,66</sup>. The second is Shapiro steps similar to those found for skyrmions and vortices under ac and dc drives on a 1D periodic substrate<sup>60</sup>. These two effects can interfere with each other. In some cases, we find a constant skyrmion Hall angle accompanied by steps in both the parallel and perpendicular velocity components, while in other cases, a series of steps in the skyrmion Hall angle coexists with regimes in which the skyrmion Hall angle is non-monotonic and either increases, decreases, or reverses sign as a function of the applied drive. We also show that for fixed dc driving, the skyrmion Hall angle can be controlled by changing the amplitude of the ac drive.

## II. SIMULATION

We consider a two-dimensional  $L \times L$  system with periodic boundary conditions and model a single skyrmion moving over a square obstacle array with lattice constant  $a$ . In Fig. 1 we show a schematic of the system highlighting the obstacles and the skyrmion trajectory for a dc drives  $F^D$  applied along the  $x$ -direction. We apply an additional ac drive along the  $x$ -direction, as shown in Fig. 1(a), or along the  $y$ -direction, as illustrated in Fig. 1(b). In the presence of only a dc drive, a series of directional locking steps appear due to the velocity dependence of the skyrmion Hall effect<sup>66</sup>.

We use a particle based model for skyrmions interacting with disorder<sup>31,36,37,66,67</sup>. The equation of motion for skyrmion  $i$  is:

$$\alpha_d \mathbf{v}_i + \alpha_m \hat{\mathbf{z}} \times \mathbf{v}_i = \mathbf{F}^{obs} + \mathbf{F}^D + \mathbf{F}^{AC} \quad (1)$$

The first term  $\alpha_d$  on the left is the damping term, and the second term  $\alpha_m$  is the Magnus force, which produces velocities that are perpendicular to the net force experienced by the skyrmion. Unless otherwise noted, we

normalize the damping and Magnus coefficients so that  $\alpha_d^2 + \alpha_m^2 = 1$ .

The first term on the right,  $\mathbf{F}^{obs}$ , represents the interaction between the skyrmion and the obstacles. The potential energy of this interaction has a Gaussian form  $U_o = C_o e^{-(r_{io}/a_o)^2}$ , where  $C_o$  is the strength of the obstacle potential,  $r_{io}$  is the distance between skyrmion  $i$  and obstacle  $o$ , and  $a_o$  is the obstacle radius. The force between an obstacle and the skyrmion is given by  $\mathbf{F}_i^o = -\nabla U_o = -F_o r_{io} e^{-(r_{io}/a_o)^2} \hat{\mathbf{r}}_{io}$ , where  $F_o = 2U_o/a_o^2$ . For computational efficiency, we place a cut-off on the obstacle interaction at  $r_{io} = 2.0$  since the interaction becomes negligible beyond this distance. We set the obstacle density to  $\rho_o = 0.093/\xi^2$  and the obstacle radius to  $a_o = 0.65$ . The dc drive is represented by the term  $\mathbf{F}^D = F^D \hat{\mathbf{x}}$ . We increase the dc drive in small increments of  $\delta F^D = 0.001$ , and we wait  $10^5$  simulation time steps between increments to ensure that the system has reached a steady state. The ac drive has the form  $\mathbf{F}^{AC} = A \sin(\omega t) \hat{\mathbf{a}}$  for driving in the  $x$  ( $\hat{\mathbf{a}} = \hat{\mathbf{x}}$ ) or  $y$  ( $\hat{\mathbf{a}} = \hat{\mathbf{y}}$ ) direction. Here  $A$  is the amplitude of the ac drive and the drive frequency is  $\omega = 2 \times 10^{-4}$  inverse simulation steps. We measure the skyrmion velocity parallel,  $\langle V_{\parallel} \rangle = \langle \mathbf{v}_i \cdot \hat{\mathbf{x}} \rangle$ , and perpendicular,  $\langle V_{\perp} \rangle = \langle \mathbf{v}_i \cdot \hat{\mathbf{y}} \rangle$ , to the dc drive. In the absence of any obstacles, the skyrmion moves at the intrinsic skyrmion Hall angle,  $\theta_{sk}^{int} = \arctan(\alpha_m/\alpha_d)$ . We can also quantify the dynamics by measuring  $R = \langle V_{\perp} \rangle / \langle V_{\parallel} \rangle$ , where the skyrmion Hall angle is given by  $\theta_{sk} = \arctan(R)$ .

### III. DC AND AC DRIVE IN THE SAME DIRECTION

We first consider the case where the ac drive is applied along the same direction as the dc drive,  $\mathbf{F}^{AC} = A \sin(\omega t) \hat{\mathbf{x}}$ . For an overdamped particle moving over a periodic array, this drive configuration produces Shapiro steps in the velocity-force curves, and the motion is strictly in the drive direction, giving a Hall angle of zero. In Fig. 2(a) we plot  $\langle V_{\perp} \rangle$  and  $\langle V_{\parallel} \rangle$  versus  $F^D$  at zero ac driving,  $A = 0.0$ , in a sample with  $\alpha_m/\alpha_d = 0.45$ , while in Fig. 2(b) we show the corresponding  $\theta_{sk}$  versus  $F^D$  curve. A series of jumps in the velocity-force curves are associated with different locking directions for the skyrmion motion, as indicated by the jumps in  $\theta_{sk}$ . This is a result of the pinning-induced velocity dependence of the skyrmion Hall angle, as previously studied for skyrmions moving over a periodic pinning or obstacle array<sup>36,66</sup>.

When a finite ac drive of  $A = 0.5$  is applied along the  $x$  direction in the same system, the behavior changes as illustrated in Fig. 3. In Fig. 3(a) we plot  $\langle V_{\parallel} \rangle$  and  $\langle V_{\perp} \rangle$  versus  $F^D$ , while in Fig. 3(b) we show the corresponding  $\theta_{sk}$  versus  $F^D$  curve. The skyrmion motion is initially locked along the  $x$ -direction for  $F^D < 0.65$ , and above this drive  $\langle V_{\perp} \rangle$  begins to increase in a series of steps. The skyrmion Hall is non-monotonic between the steps.

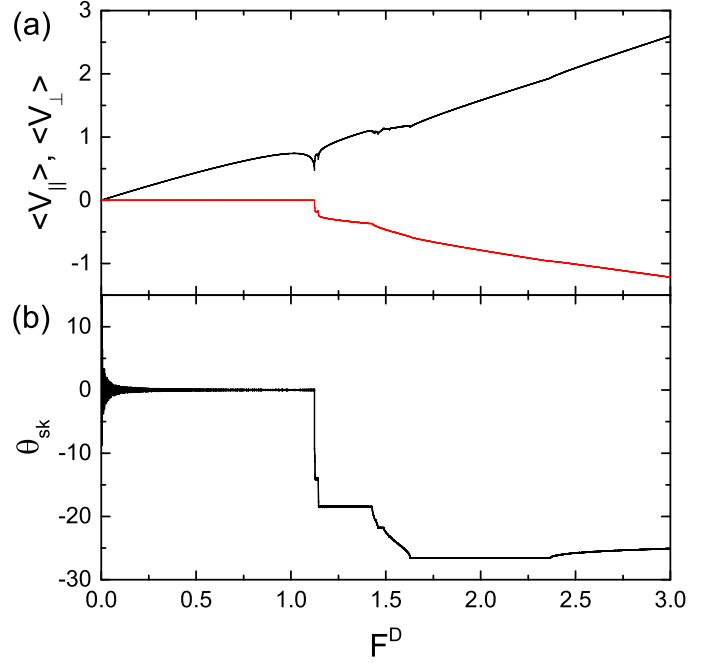


FIG. 2.  $\langle V_{\perp} \rangle$  (red) and  $\langle V_{\parallel} \rangle$  (black) vs  $F^D$  for strictly dc driving with an ac drive amplitude of  $A = 0.0$  in a sample with  $\alpha_m/\alpha_d = 0.45$ . (b) The corresponding  $\theta_{sk}$  vs  $F^D$ .

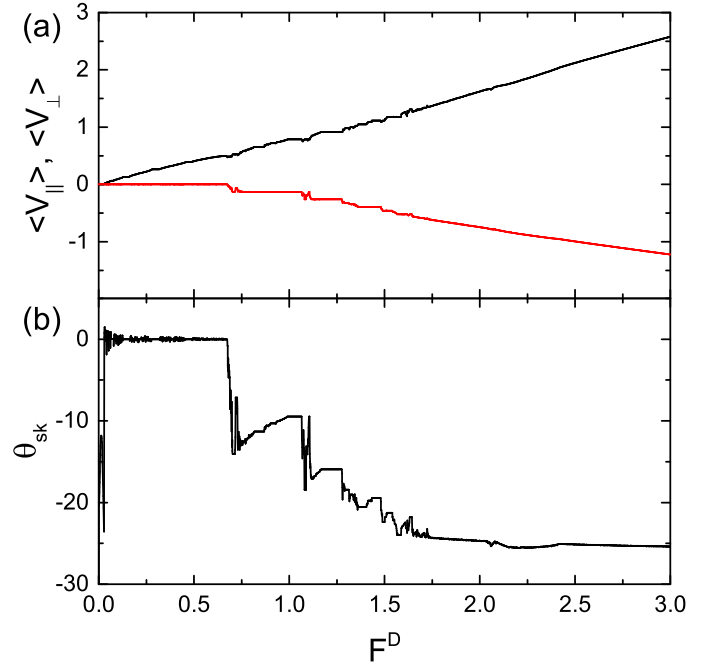


FIG. 3. (a)  $\langle V_{\parallel} \rangle$  (black) and  $\langle V_{\perp} \rangle$  (red) vs  $F^D$  for the system in Fig. 2 with  $\alpha_m/\alpha_d = 0.45$  under a finite ac drive with  $A = 0.5$  applied along the  $x$  direction. (b) The corresponding  $\theta_{sk}$  vs  $F^D$ . There are windows of drive over which the magnitude of  $\theta_{sk}$  decreases with increasing  $F^D$ .

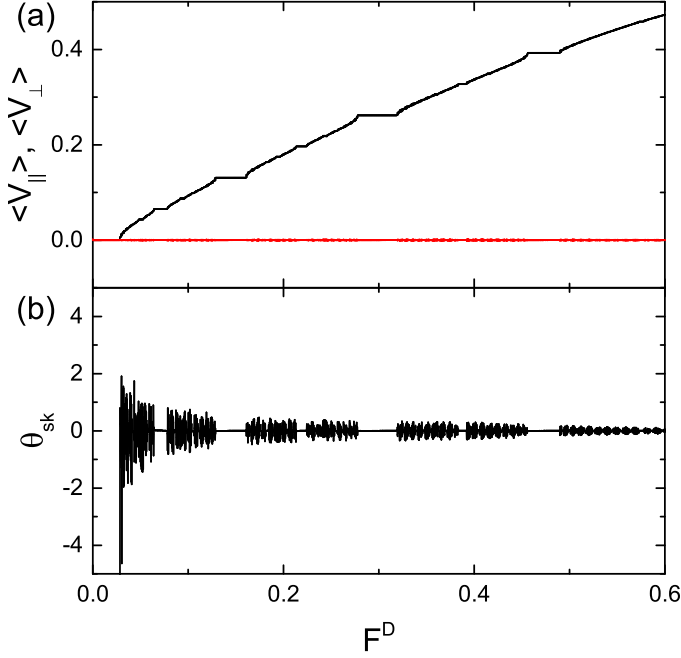


FIG. 4. (a)  $\langle V_{||} \rangle$  (black) and  $\langle V_{\perp} \rangle$  (red) vs  $F^D$  for the system in Fig. 3 with  $\alpha_m/\alpha_d = 0.45$  and  $x$  direction ac driving of  $A = 0.5$  zoomed in on the range  $0.0 < F^D < 0.6$ . (b) The corresponding  $\theta_{sk}$  vs  $F^D$  showing Shapiro steps.

Above the first step in  $\langle V_{\perp} \rangle$ , the Hall angle is close to  $\theta_{sk} = -12.5^\circ$ , and it decreases in magnitude with increasing drive to  $\theta_{sk} = -8^\circ$  before increasing in magnitude again. This pattern repeats several times until, at high drives,  $\theta_{sk}$  saturates to  $\theta_{sk} = 24^\circ$ , a value close to the pin-free intrinsic skyrmion Hall angle. At the higher drives, the steps in the velocity force curves also become smoother. The decreases in magnitude of the skyrmion Hall angle with increasing  $F^D$  have not been observed for skyrmions interacting with random pinning.

In Fig. 4(a,b), we zoom in on the range  $0 < F^D < 0.6$  for the two velocity components and  $\theta_{sk}$  in the system from Fig. 3. Here  $\theta_{sk} = 0.0$  and  $\langle V_{\perp} \rangle = 0$ , indicating that the motion is locked along  $x$  direction; however, a set of phase locking steps still appear in  $\langle V_{||} \rangle$ . These are Shapiro steps, which also occur in the overdamped limit. The steps correspond to windows of drive over which  $\langle V_{||} \rangle$  is locked to a constant value. In contrast, the directional locking found in the absence of an ac drive in Fig. 2 is not associated with constant velocity steps but instead is accompanied by dips and cusps in the velocities.

Figure 5(a,b) shows the curves from Fig. 3 over the interval  $0.7 < F^D < 1.2$ , where we find two new features. The first is that  $\langle V_{\perp} \rangle$  has a fixed finite value, indicating that the particle is moving at an angle to the dc drive. The second is that the series of steps which appear in  $\langle V_{||} \rangle$  are correlated with steps in  $\theta_{sk}$ , which is *decreasing* in magnitude as  $F^D$  increases. This indicates that the velocity is increasing in the  $x$  direction but remains constant in the  $y$  direction, and the different phase locking

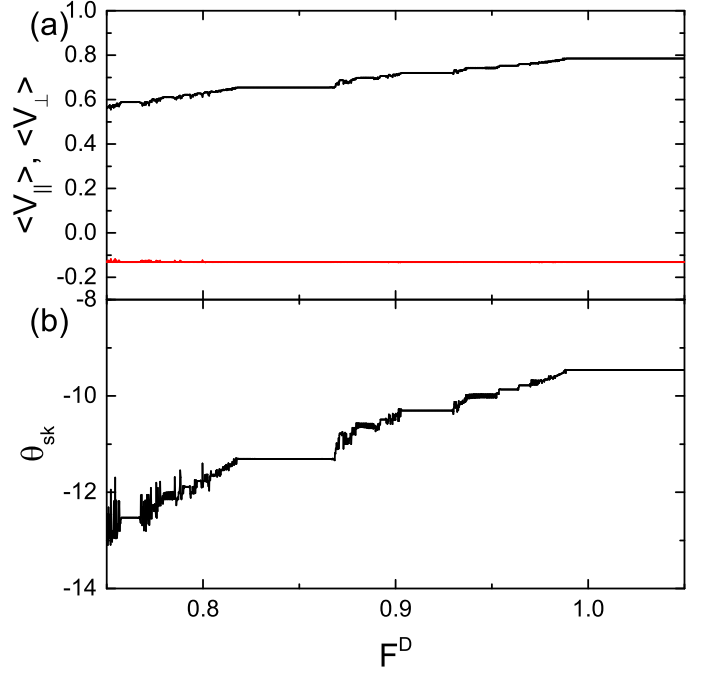


FIG. 5. (a)  $\langle V_{||} \rangle$  (black) and  $\langle V_{\perp} \rangle$  (red) vs  $F^D$  for the system in Fig. 3 with  $\alpha_m/\alpha_d = 0.45$  and  $x$  direction ac driving of  $A = 0.5$  zoomed in on the range  $0.7 < F^D < 1.2$ . (b) The corresponding  $\theta_{sk}$  vs  $F^D$ , showing a regime of decreasing skyrmion Hall angle magnitude.

steps are associated with decreases in the magnitude of the skyrmion Hall angle. Near  $F^D = 1.2$  in Fig. 3, there is a substantial jump in  $\theta_{sk}$  to a larger magnitude which coincides with a jump to a new step in  $\langle V_{\perp} \rangle$ .

The results in Figs. 3, 4, and 5 show that the phase locking behavior found in Fig. 3 is actually a *mixture* of two different types of locking. The first is the Shapiro step phase locking associated with the matching of the ac drive frequency or its higher harmonics to the increasing frequency of the skyrmion velocity oscillations caused by the periodic collisions with the obstacles under an increasing dc drive. This locking is associated with a  $\theta_{sk}$  value that is either constant or increasing in magnitude. The second is the directional locking which occurs even in the absence of an ac drive, as shown in Fig. 2 and observed in previous works<sup>36,53,66</sup>. These two locking phenomena can interact with each other to create regions where the magnitude of the skyrmion Hall angle is either constant or decreasing with drive instead of increasing with drive. We note that directional locking effects for a particle moving over a periodic substrate can also occur for overdamped systems such as vortices in type-II superconductors moving over 2D pinning arrays<sup>68,69</sup> and colloids moving over optical traps<sup>69-74</sup> or periodic substrates<sup>75,76</sup>; however, in those systems the direction of the drive with respect to the substrate must be varied, whereas for the skyrmions, the velocity dependence of the skyrmion Hall angle changes the direction of motion even when the driving direction is fixed<sup>36,66</sup>.



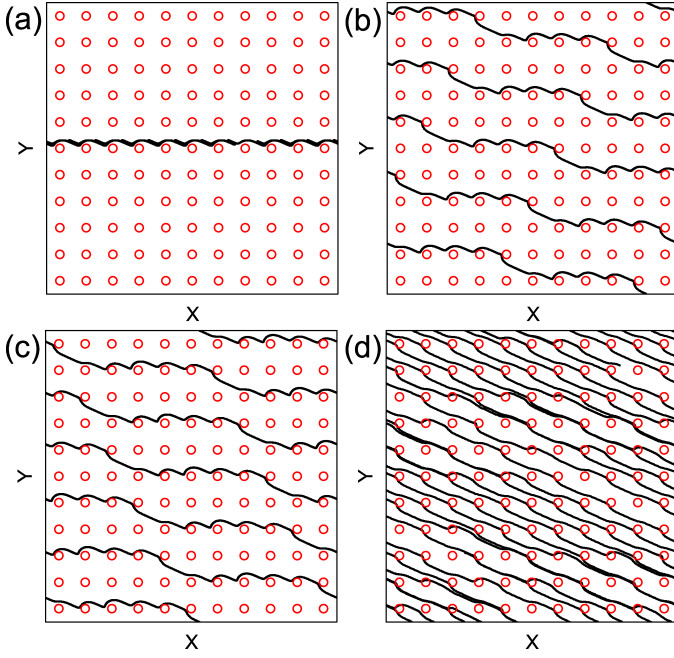


FIG. 6. Skymion trajectory (black line) and obstacle locations (red circles) for the system in Fig. 3 with  $\alpha_m/\alpha_d = 0.45$  and  $x$  direction ac driving with  $A = 0.5$ . (a)  $F^D = 0.3$  where the motion is locked in the  $x$  direction. (b)  $F^D = 0.85$  where there is finite motion along  $y$  with  $\theta_{sk} = -11.3^\circ$ . (c)  $F^D = 1.0$ , where  $\theta_{sk} = -8.1^\circ$ . (d)  $F^D = 2.0$ , where  $\theta_{sk} = -22^\circ$ .

In Fig. 6(a) we plot the skymion trajectories for the system in Fig. 3 at  $F^D = 0.3$  where the skymion motion is locked in the  $x$ -direction with  $\theta_{sk} = 0^\circ$ . At  $F^D = 0.85$  in Fig. 6(b), the skymion has a finite displacement in the negative  $y$ -direction and it traverses five obstacles in the  $x$ -direction for every one obstacle in the  $y$  direction, giving a ratio of  $R = 1/5$  and  $\theta_{sk} = \arctan(1/5) = -11.3^\circ$ . In Fig. 6(c) at  $F^D = 1.0$ , the velocity in the  $y$ -direction is unchanged but the skymion Hall angle has a smaller magnitude of  $-8.1^\circ$ , and the skymion moves 7 lattice constants in  $x$  and one lattice constant in  $y$  during a single ac drive period. Figure 6(d) shows the trajectories in the same system at  $F^D = 2.0$ , where  $\theta_{sk}$  is close to  $\theta_{sk} = -22^\circ$ . Here the system is not on a locking step and the trajectories are more disordered.

In Fig. 7(a) we plot  $\langle V_{||} \rangle$  and  $\langle V_{\perp} \rangle$  versus  $F_D$  for a system with  $x$  direction ac driving of magnitude  $A = 0.5$  as in Fig. 3 but with  $\alpha_m/\alpha_d = 1.0$ , where the intrinsic Hall angle is  $\theta_{sk}^{int} = 45^\circ$ . Figure 7(b) shows the corresponding measured  $\theta_{sk}$  which has only two values, with  $\theta_{sk} = 0^\circ$  at small drives followed by a jump to the intrinsic value  $\theta_{sk} = -45^\circ$ , indicating that there are no intermediate directional locking phases. Once the system is locked to  $-45^\circ$ , a series of Shapiro steps still appear in both the parallel and perpendicular velocities in Fig. 7(a) that do not correspond to changes in  $\theta_{sk}$ . This shows that it is possible for Shapiro steps to occur even when the system motion is fixed along a locking angle. On the Shapiro

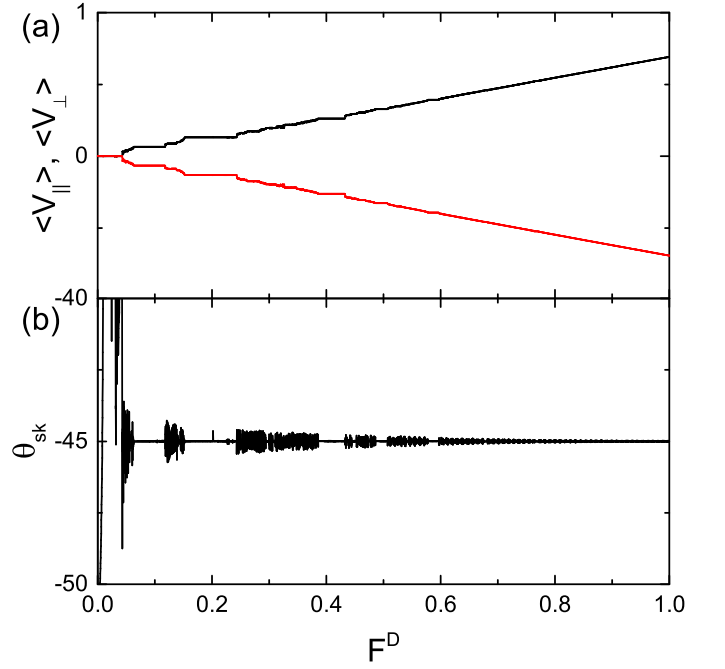


FIG. 7. (a)  $\langle V_{||} \rangle$  (black) and  $\langle V_{\perp} \rangle$  (red) vs  $F_D$  for a system with  $x$  direction ac driving of magnitude  $A = 0.5$  at  $\alpha_m/\alpha_d = 1.0$ , where the intrinsic Hall angle is  $\theta_{sk}^{int} = 45^\circ$ . (b) The corresponding  $\theta_{sk}$  vs  $F_D$ . Here the motion is locked to  $45^\circ$  but there is still a series of Shapiro steps that are not associated with a changing skymion Hall angle.

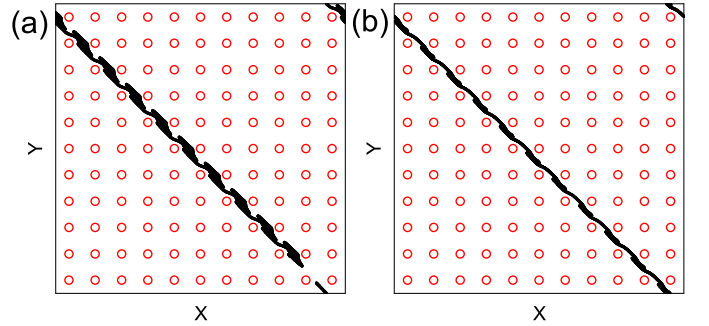


FIG. 8. Skymion trajectory (black line) and obstacle locations (red circles) for the system in Fig. 7 with  $\alpha_m/\alpha_d = 1.0$  and  $x$  direction ac driving of magnitude  $A = 0.5$ . (a)  $F_D = 0.1$ , where the trajectories are partially disordered. (b) Along a step at  $F_D = 0.2$ , where the trajectories are more ordered.

steps in Fig. 7, the skymion trajectories are much more ordered, as shown in Fig. 8(b) at  $F_D = 0.2$ , while for  $F_D = 0.1$  in Fig. 8(a), the trajectories are less ordered. In general, we find that if the ratio  $\alpha_m/\alpha_d$  produces an intrinsic skymion Hall angle that gives a ratio of  $y$  to  $x$  motion that is close to  $1/4, 1/3, 1/2$ , or  $1$ , which correspond to strong symmetry directions of the substrate lattice, the system locks permanently to this symmetry direction even for very low drives, and steps in the velocity appear that are a signature of Shapiro steps instead

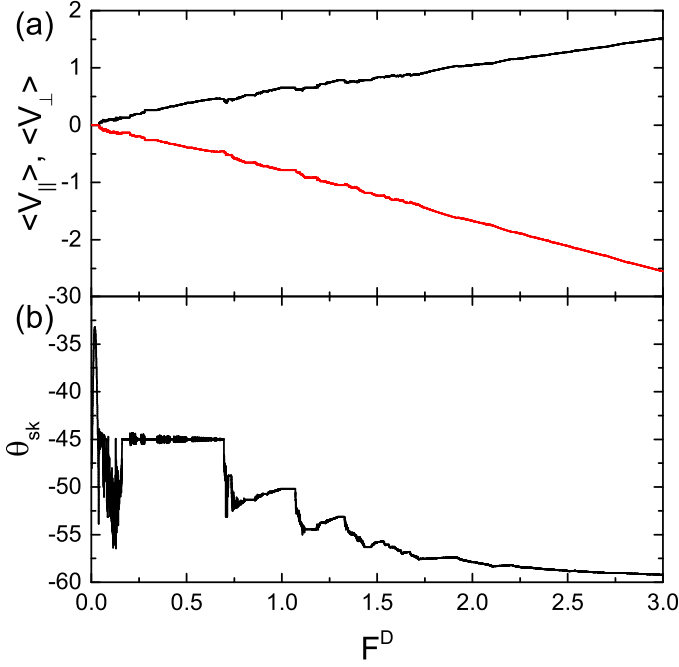


FIG. 9. (a)  $\langle V_{\parallel} \rangle$  (black) and  $\langle V_{\perp} \rangle$  (red) vs  $F^D$  for a system with  $x$  direction ac driving of magnitude  $A = 0.5$  at  $\alpha_m/\alpha_d = 1.732$ . (b) The corresponding  $\theta_{sk}$  vs  $F^D$ .

of directional locking steps.

In Fig. 9(a) we plot  $\langle V_{\parallel} \rangle$  and  $\langle V_{\perp} \rangle$  versus  $F^D$  for a system with  $x$  direction ac driving of magnitude  $A = 0.5$  as in Fig. 3 but with  $\alpha_m/\alpha_d = 1.732$ , giving an intrinsic Hall angle of  $\theta_{sk} = 60^\circ$ . Figure 9(b) shows the corresponding  $\theta_{sk}$  versus  $F^D$ . Here the system is directionally locked to  $\theta_{sk} = 45^\circ$ , but there is still a series of steps in the velocities at low  $F^D$  despite the fact that the Hall angle is constant in this regime. For  $F^D > 0.6$ , a series of steps appear in  $\theta_{sk}$  as the system switches between different locking steps. The larger increases in the magnitude of  $\theta_{sk}$  are followed by regions in which the magnitude of  $\theta_{sk}$  decreases by a smaller amount, and at large  $F^D$ ,  $\theta_{sk}$  gradually approaches the intrinsic value. In Fig. 10(a) we illustrate the skyrmion trajectory for the system in Fig. 9 at  $F^D = 0.5$  where the skyrmion is in the  $\theta_{sk} = -45^\circ$  directional locking regime, while in Fig. 10(b) we show the  $F^D = 1.0$  state where the skyrmion is locked to an angle close to  $\theta_{sk} = -50^\circ$ . At  $F^D = 1.3$  in Fig. 10(c), the skyrmion is moving in an alternating fashion. In Fig. 10(d) at  $F^D = 1.75$ ,  $\theta_{sk} = -57.5^\circ$ .

For increasing Magnus force, the dynamics become increasingly disordered, weakening both the directional locking and the Shapiro steps. Figure 11(a) shows  $\langle V_{\parallel} \rangle$  and  $\langle V_{\perp} \rangle$  versus  $F^D$  for a system with  $x$  direction ac driving at  $A = 0.5$ , as in Fig. 9, but for  $\alpha_m/\alpha_d = 9.962$ , where the intrinsic Hall angle is  $\theta_{sk} = 84.3^\circ$ . Figure 11(b) shows the corresponding  $\theta_{sk}$  versus  $F^D$ . In this case there are only small steps in the velocity force curves that are associated with steps in  $\theta_{sk}$ , which has an average value near  $\theta_{sk} = -82.5^\circ$ . For these higher Magnus forces, the

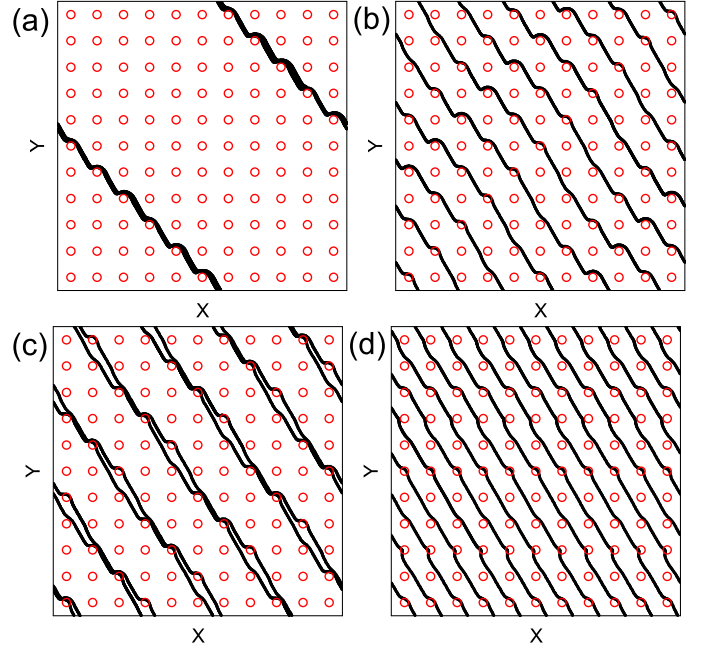


FIG. 10. Skyrmion trajectory (black line) and obstacle locations (red circles) for the system in Fig. 9 with  $\alpha_m/\alpha_d = 1.732$  and  $x$  direction ac driving of magnitude  $A = 0.5$ . (a)  $F^D = 0.5$ , where the system is locked to  $\theta_{sk} = -45^\circ$ . (b)  $F^D = 1.0$ . (c)  $F^D = 1.3$ . (d)  $F^D = 1.75$  with  $\theta_{sk} = -57.5^\circ$ .

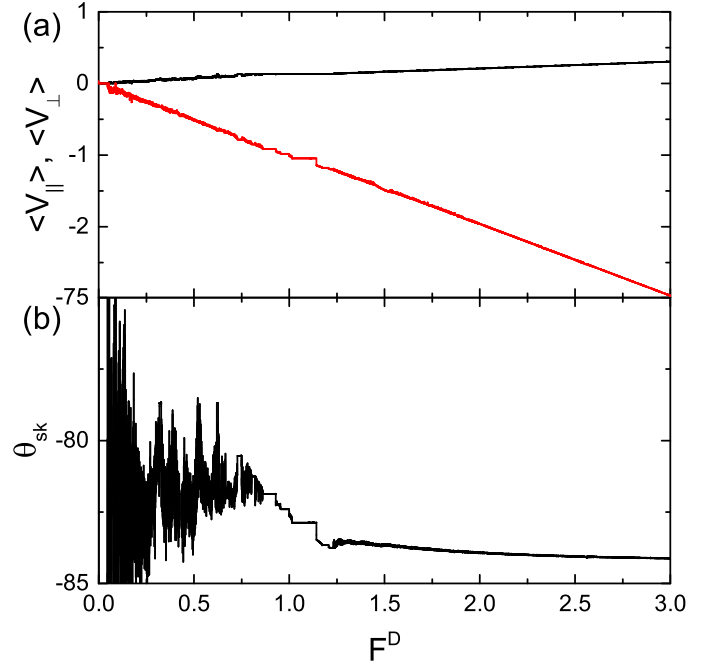


FIG. 11. (a)  $\langle V_{\parallel} \rangle$  (black) and  $\langle V_{\perp} \rangle$  (red) vs  $F^D$  for a system with  $x$  direction ac driving of magnitude  $A = 0.5$  at  $\alpha_m/\alpha_d = 9.962$ . (b) The corresponding  $\theta_{sk}$  vs  $F^D$ .

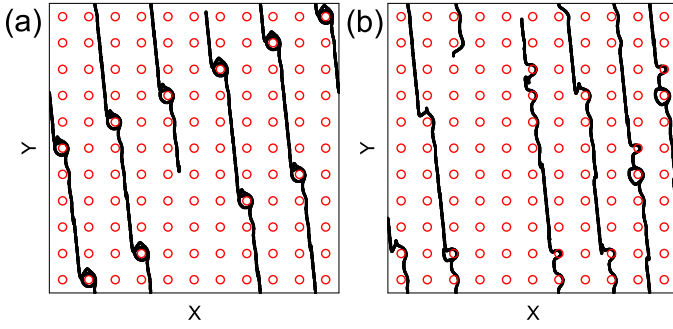


FIG. 12. Skymion trajectory (black line) and obstacle locations (red circles) for the system in Fig. 12 with  $\alpha_m/\alpha_d = 9.962$ ,  $x$  direction ac driving, and  $A = 0.5$ . (a) At  $F_D = 0.33$ , loop orbits appear. (b) At  $F_D = 0.5$ , the orbits are disordered.

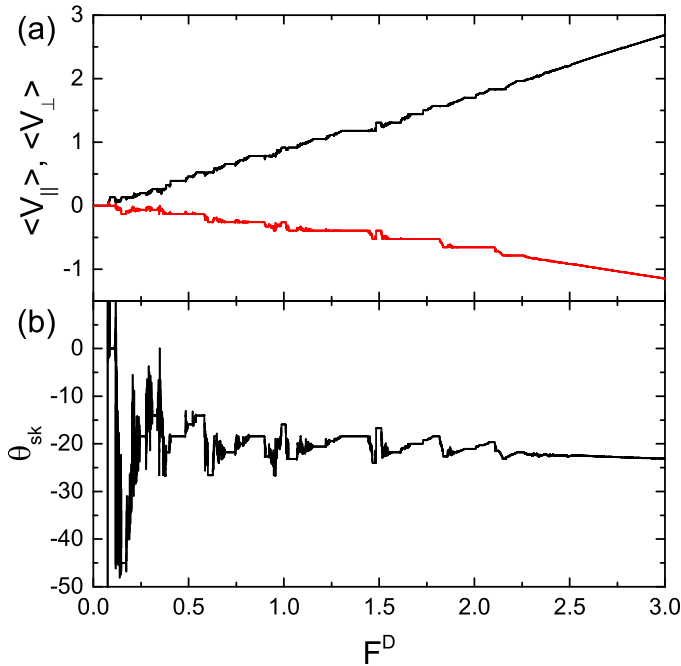


FIG. 13. (a)  $\langle V_{\parallel} \rangle$  (black) and  $\langle V_{\perp} \rangle$  (red) for a system with  $\alpha_m/\alpha_d = 0.45$  and  $y$  direction ac driving of magnitude  $A = 0.5$ . (b) The corresponding  $\theta_{sk}$  vs  $F^D$ . We find more steps than for the same system with ac driving in the  $x$  direction (Fig. 3).

skymion starts to perform full or partial loops around the obstacles, as shown in Fig. 12(a) at  $F_D = 0.33$ . In Fig. 12(b) at  $F_D = 0.5$ , the system is in a disordered phase. For  $F_D > 1.5$ , the locking regimes are lost and  $\theta_{sk}$  gradually approaches the intrinsic Hall angle value.

#### IV. AC DRIVING IN THE TRANSVERSE DIRECTION

We next consider the case where the ac drive is applied along the  $y$ -direction, transverse to the dc drive.

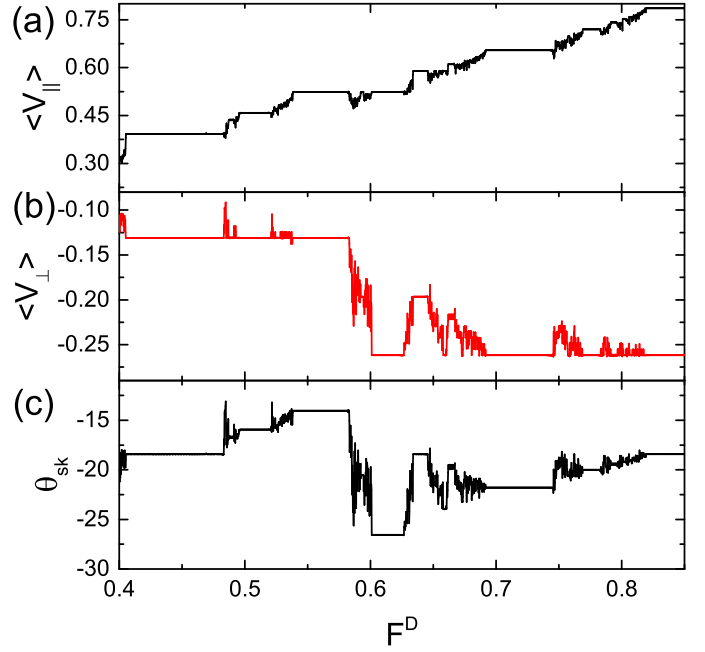


FIG. 14. (a)  $\langle V_{\parallel} \rangle$ , (b)  $\langle V_{\perp} \rangle$ , and (c)  $\theta_{sk}$  vs  $F_D$  for the system in Fig. 13 with  $\alpha_m/\alpha_d = 0.45$ ,  $A = 0.5$ , and  $y$  direction ac driving shown over the interval  $0.4 < F^D < 0.85$ .

In Fig. 13(a) we plot the velocity components versus  $F^D$  and in Fig. 13(b) we show the corresponding  $\theta_{sk}$  versus  $F^D$  for a system with  $\alpha_m/\alpha_d = 0.45$  and  $A = 0.5$ . The features in the velocity curves are more step like, rather than the cusp like shapes found for  $x$  direction ac driving in Fig. 3, and in general there are more locking regions which are associated with both directional locking and the ac phase locking. Another interesting feature is that near  $F^D = 0.15$ , there is a window of locking to  $\theta_{sk} = -45^\circ$ , which is considerably larger in magnitude than the intrinsic skymion Hall angle of  $\theta_{sk} = 24.2^\circ$ . We call this a Hall angle overshoot. As  $F_D$  increases,  $\theta_{sk}$  undergoes a number of oscillations until it reaches a saturation near the intrinsic value at high  $F^D$ . In Fig. 14 we plot  $\langle V_{\parallel} \rangle$ ,  $\langle V_{\perp} \rangle$ , and  $\theta_{sk}$  versus  $F^D$  for the system in Fig. 13 over the interval  $0.4 < F^D < 0.85$ . There are sudden jumps both up and down in  $\theta_{sk}$ . Additionally, there are regions where  $\langle V_{\perp} \rangle$  remains constant but steps appear in  $\langle V_{\parallel} \rangle$  that are associated with jumps in  $\theta_{sk}$ . In the interval  $1.35 < F^D < 1.75$  shown in Fig. 15(a,b,c), there are regions where the velocity can decrease with increasing  $F_D$ .

In Fig. 16 we show some of the representative skymion orbits for the system in Fig. 13. At  $F^D = 0.1$  in Fig. 16(a), the motion is locked in the  $x$  direction, and the skymion executes a zig-zag pattern. In Fig. 16(b) at  $F^D = 0.16$ , the motion is locked to  $\theta_{sk} = -45^\circ$ . Figure 16(c) shows the trajectory at  $F^D = 0.26$ , where the skymion moves at a much smaller angle of  $\theta_{sk} \approx -18.4^\circ$ . In Fig. 16(d) at  $F^D = 0.44$ , we still find  $\theta_{sk} = 18.4^\circ$  but the orbit shape has changed, with the skymion moving

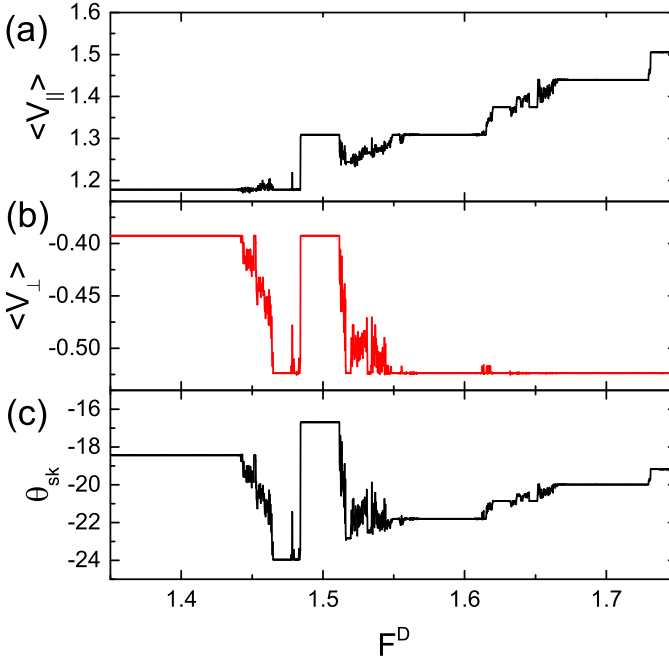


FIG. 15. (a)  $\langle V_{||} \rangle$ , (b)  $\langle V_{\perp} \rangle$ , and (c)  $\theta_{sk}$  vs  $F^D$  for the system in Fig. 13 with  $\alpha_m/\alpha_d = 0.45$ ,  $A = 0.5$ , and  $y$  direction ac driving shown over the interval  $1.35 < F^D < 1.75$ .

$3a$  in the  $x$  direction and  $a$  in the  $y$  direction during each ac drive cycle. At  $F^D = 0.61$  in Fig. 16(e), the motion is along  $\theta_{sk} = -26.6^\circ$ , and in Fig. 16(f) at  $F^D = 1.4$ ,  $\theta_{sk} = -18.4^\circ$ , indicating that the system has returned to the  $1/3$  locking region. The orbit differs from that shown in Fig. 16(d), indicating that  $R = 1/3$  locking can occur in several different ways.

In Fig. 17(a) we plot the velocity curves versus  $F^D$  and in Fig 17(b) we show the corresponding  $\theta_{sk}$  versus  $F^D$  for a system with  $\alpha_m/\alpha_d = 1.732$ , where there are again a series of steps at which  $\theta_{sk}$  increases or decreases. Locking occurs in several regimes and the system jumps in and out of the  $\theta_{sk} = -45^\circ$  locked state since the  $45^\circ$  locking is a particularly strong symmetry direction of the square obstacle lattice. In Fig. 18(a,b) we plot the skyrmion trajectories for the system in Fig. 17 at  $F^D = 0.15$  in the  $-45^\circ$  locking regime and at  $F^D = 0.185$ , where the skyrmions move at a lower magnitude angle of  $\theta_{sk} = -33.7^\circ$ . In Fig. 18(c) at  $F^D = 0.3$ , the system jumps to a new  $-45^\circ$  locking phase with a braiding pattern, and in Fig. 18(d) at  $F^D = 0.43$ , the motion is along  $\theta_{sk} = -56.3^\circ$ .

For higher values of  $\alpha_m/\alpha_d$ , we again observe extended regions in which the trajectories are disordered, and the phase locking phenomena is generally reduced. In Fig. 19 we show the velocities and skyrmion Hall angle versus  $F^D$  for a system with  $A = 0.5$  and  $y$  direction ac driving as in Fig. 17 but for  $\alpha_m/\alpha_d = 9.962$ . There are a number of smaller steps, particularly in the range  $0.35 < F^D < 1.0$ , along with one larger step near  $F^D = 2.5$ . Figure 20(a) illustrates the skyrmion trajectories for the system in Fig. 19 at  $F^D = 0.25$ , where there is no phase locking

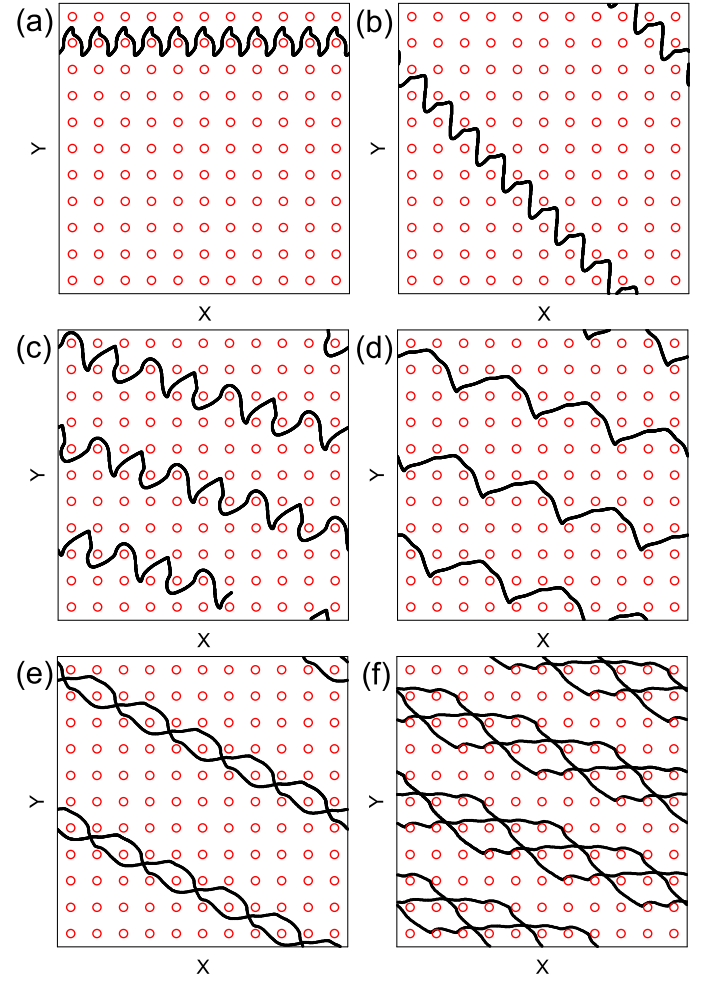


FIG. 16. Skyrmion trajectory (black line) and obstacle locations (red circles) for the system in Fig. 13 with  $\alpha_m/\alpha_d = 0.45$ ,  $A = 0.5$ , and  $y$  direction ac driving. (a) At  $F^D = 0.1$  the motion is aligned with the  $x$  direction. (b) At  $F^D = 0.16$ , the motion is locked to  $\theta_{sk} = -45^\circ$ . (c) At  $F^D = 0.26$ , the motion is at a smaller angle of  $\theta_{sk} = -18.4^\circ$ . (d)  $F^D = 0.44$ . (e)  $F^D = 0.61$ . (f)  $F^D = 1.4$ .

state and the trajectories form a non-repeating pattern. In Fig. 20(b) at  $F^D = 0.465$ , the system is phase locked at  $\theta_{sk} = -76^\circ$  and the trajectories are ordered.

For ac driving in the  $y$ -direction, there is an interplay between three types of phase locking. These are the Shapiro steps, the directional locking, and the transverse phase locking effect. This is the reason that there are a larger number of steps in the velocity and skyrmion Hall angle curves compared to ac driving in the  $x$  direction.

### A. Hall Angle Reversal

In most cases, we have shown that although the skyrmion Hall angle increases or decreases with drive, it maintains the same sign. Under certain circumstances, however, we find regions in which the skyrmion Hall angle

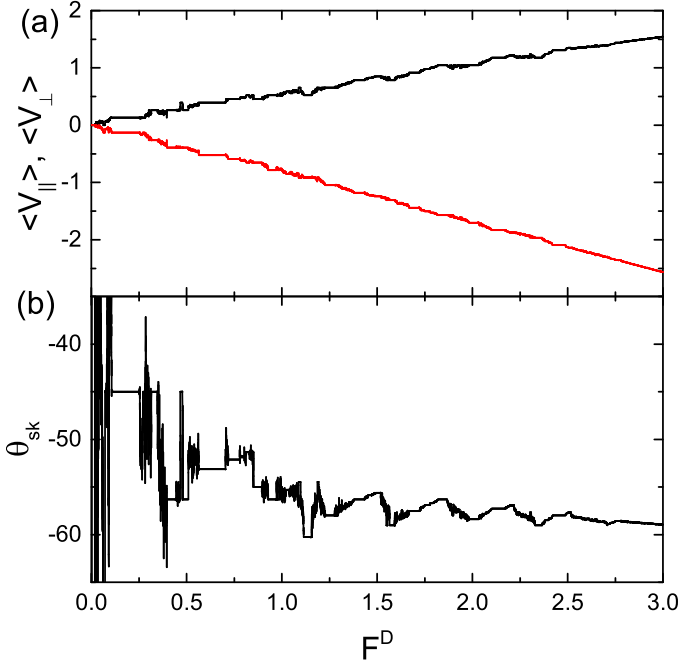


FIG. 17. (a)  $\langle V_{||} \rangle$  (black) and  $\langle V_{\perp} \rangle$  (red) vs  $F^D$  for a system with  $\alpha_m/\alpha_d = 1.732$ ,  $A = 0.5$ , and  $y$  direction ac driving. (b) The corresponding  $\theta_{sk}$  vs  $F^D$ .

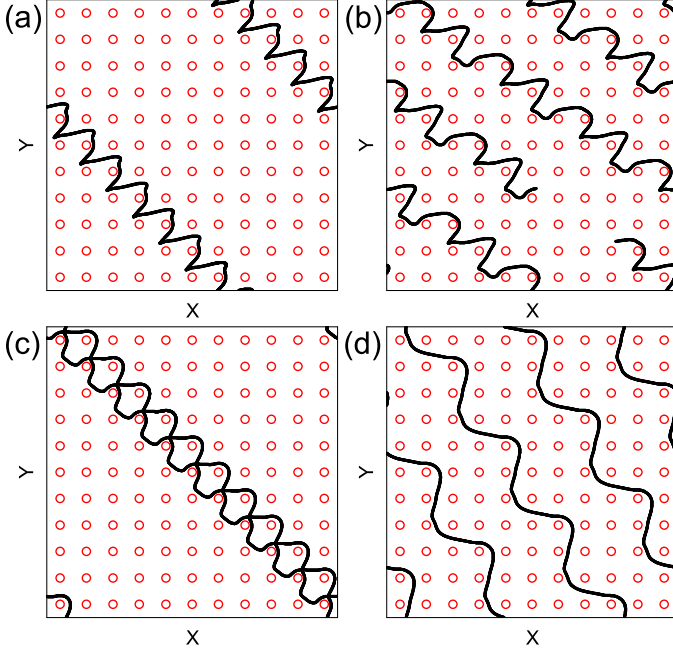


FIG. 18. Skymion trajectory (black line) and obstacle locations (red circles) for the system in Fig. 17 with  $\alpha_m/\alpha_d = 1.732$ ,  $A = 0.5$ , and  $y$  direction ac driving. (a) At  $F^D = 0.15$ , the motion is locked to  $\theta_{sk} = -45^\circ$ . (b) At  $F^D = 0.175$ , the motion locks to  $\theta_{sk} = -33^\circ$ . (c) At  $F^D = 0.3$ , the motion is along  $\theta_{sk} = -45^\circ$ . (d) At  $F^D = 0.43$ , the motion locks to  $\theta_{sk} = -56.3^\circ$ .

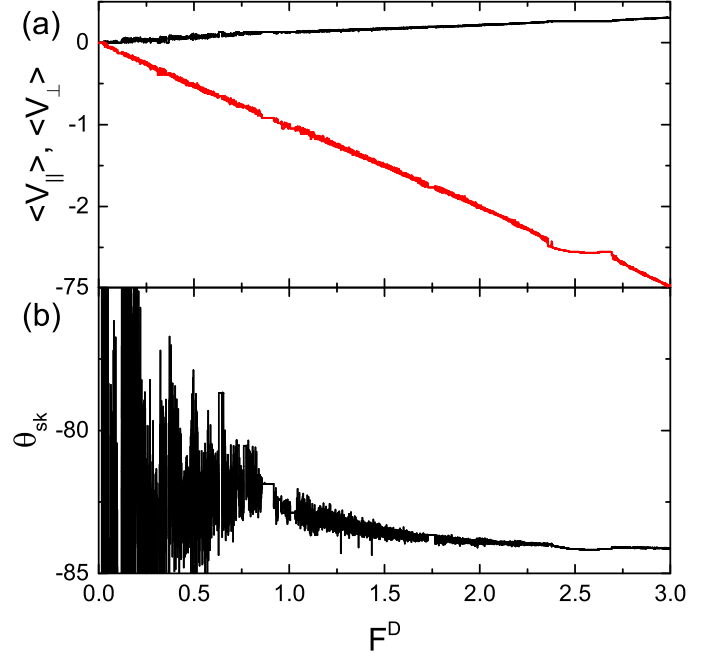


FIG. 19. (a)  $\langle V_{||} \rangle$  (black) and  $\langle V_{\perp} \rangle$  (red) vs  $F^D$  for a system with  $\alpha_m/\alpha_d = 9.962$ ,  $A = 0.5$ , and  $y$  direction ac driving. (b) The corresponding  $\theta_{sk}$  vs  $F^D$ .

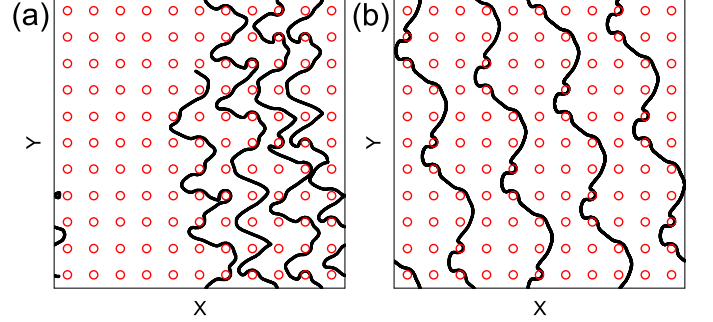


FIG. 20. Skymion trajectory (black line) and obstacle locations (red circles) for the system in Fig. 19 with  $\alpha_m/\alpha_d = 9.962$ ,  $A = 0.5$ , and  $y$  direction ac driving. (a)  $F^D = 0.25$  in a non-phase locked region. (b)  $F^D = 0.465$  in a phase locked region with  $\theta_{sk} = -76^\circ$ .

changes from positive to negative. This effect is generally associated with windows of disordered motion at smaller  $F^D$  where the skymion is jumping among different orbits. In Fig. 21 we plot  $\langle V_{||} \rangle$ ,  $\langle V_{\perp} \rangle$ , and  $\theta_{sk}$  versus  $F^D$  for a system with  $y$  direction ac driving at  $\alpha_m/\alpha_d = 1.0$ . If the ac driving were in the  $x$ -direction, this ratio of the Magnus to damping terms would produce a constant skymion Hall angle of  $\theta_{sk} = 45^\circ$  with only Shapiro steps. When the ac driving is along the  $y$  direction, however, a variety of locking regions appear that are associated with jumps both up and down in  $\langle V_{||} \rangle$  and  $\langle V_{\perp} \rangle$ . Jumps also occur in  $\theta_{sk}$  among the values  $\theta_{sk} = -45^\circ$ ,  $-38.65^\circ$ ,  $-36.87^\circ$ ,  $-33.6^\circ$ , and  $-26.56^\circ$ . The corresponding velocity ratios are  $\langle V_{\perp} \rangle / \langle V_{||} \rangle = 1, 4/5, 4/3, 2/3$ , and  $1/2$ ,



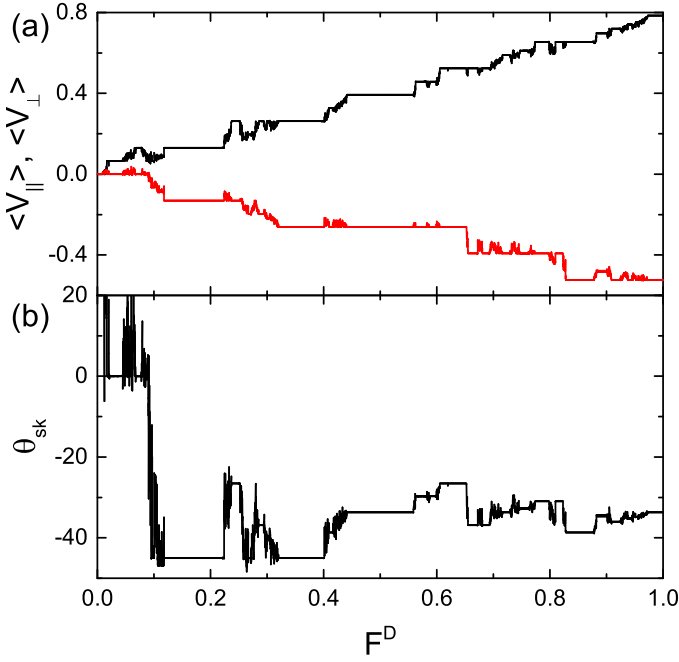


FIG. 21. (a)  $\langle V_{\parallel} \rangle$  (black) and  $\langle V_{\perp} \rangle$  (red) vs  $F^D$  for a system with  $\alpha_m/\alpha_d = 1.0$ ,  $A = 0.5$ , and  $y$  direction ac driving. (b) The corresponding  $\theta_{sk}$  vs  $F^D$ . For  $F^D < 0.1$ , there are regions in which both velocity components are positive, giving a positive skyrmion Hall angle.

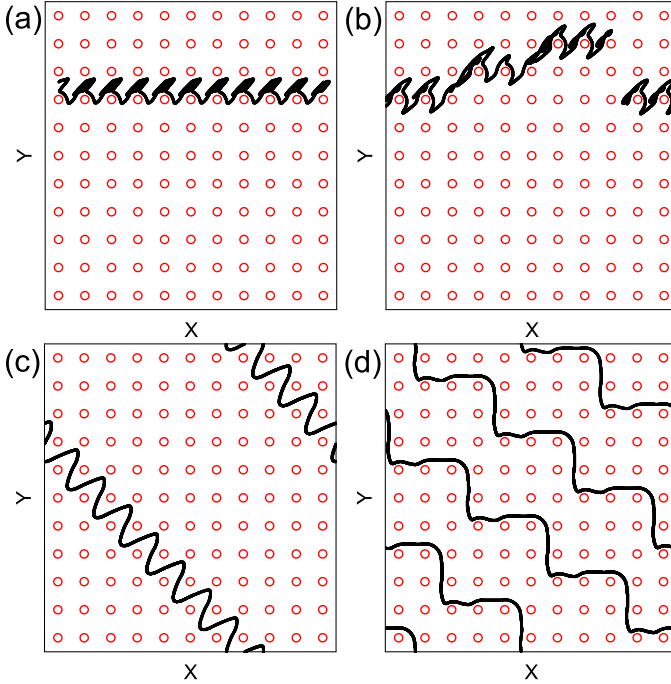


FIG. 22. Skyrmion trajectory (black line) and obstacle locations (red circles) for the system in Fig. 21 with  $\alpha_m/\alpha_d = 1.0$ ,  $A = 0.5$ , and  $y$  direction ac driving. (a) At  $F^D = 0.05$ , the motion is locked along  $x$ . (b) At  $F^D = 0.065$ , the skyrmion is also translating along the positive  $y$  direction, giving a positive skyrmion Hall angle. (c) At  $F^D = 0.2$ , there is locking at  $\theta_{sk} = -45^\circ$ . (d) At  $F^D = 0.55$  there is locking at  $\theta_{sk} = -33.7^\circ$ .

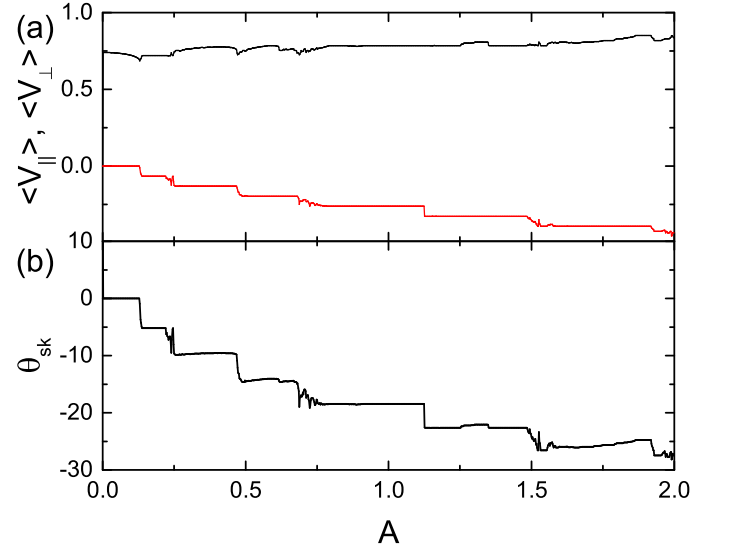


FIG. 23. (a)  $\langle V_{\parallel} \rangle$  (black) and  $\langle V_{\perp} \rangle$  (red) vs ac drive amplitude  $A$  for a system with  $\alpha_m/\alpha_d = 0.45$ , fixed  $F^D = 1.0$ , and  $x$  direction ac driving. (b) The corresponding  $\theta_{sk}$  vs  $F^D$ . Here the magnitude of the skyrmion Hall angle increases in a series of steps with increasing  $A$ .

respectively. At higher drives,  $\theta_{sk}$  decreases in magnitude to angles smaller than  $45^\circ$ . Meanwhile, for  $F^D < 0.1$  there are several regions in which  $\langle V_{\parallel} \rangle$  and  $\langle V_{\perp} \rangle$  are both finite but positive, which produces a positive skyrmion Hall angle of  $\theta_{sk} \approx 10^\circ$ . The motion in this regime is illustrated in Fig. 22(a,b) at  $F^D = 0.045$ , where the motion is locked along  $x$ , and at  $F^D = 0.065$ , where the skyrmion is jumping intermittently in the positive  $y$ -direction. Figure 22(c) shows the locking phase with  $\theta_{sk} = -45^\circ$  at  $F^D = 0.2$ , and in Fig. 22(d) at  $F^D = 0.55$ ,  $\theta_{sk} = -33.7^\circ$ . It is possible that by varying other parameters such as the size of the obstacles, clear regions of skyrmion Hall angle reversals will also emerge, but the results above indicate that such reversal effects can arise for skyrmion motion on periodic substrates.

## V. CHANGING AC AMPLITUDE

We next consider the case of a fixed dc drive of  $F^D = 1.0$  and changing ac drive amplitude  $A$  in a system with  $x$  direction ac driving at  $\alpha_m/\alpha_d = 0.45$ . In Fig. 23(a) we plot  $\langle V_{\parallel} \rangle$  and  $\langle V_{\perp} \rangle$  versus  $A$  and in Fig. 23(b) we show the corresponding  $\theta_{sk}$  versus  $A$ . When  $A = 0.0$ , the skyrmion motion is locked along the  $x$  direction, giving  $\theta_{sk} = 0$ . As  $A$  increases,  $\langle V_{\parallel} \rangle$  remains fairly constant due to the fixed value of  $F^D$ , but small cusps are present which are correlated with a series of increasing steps in  $\langle V_{\perp} \rangle$ . The steps in  $\langle V_{\perp} \rangle$  produce a series of steps in  $\theta_{sk} = \arctan(R)$  at  $R = 0, 1/10, 1/6, 1/5$ , and a small step near  $1/4$ . There are extended steps for  $R = 1/3, 3/7$ , and  $1/2$ . In general, we find that the magnitude of the Hall angle increases with increasing  $A$ . In Fig. 24(a)

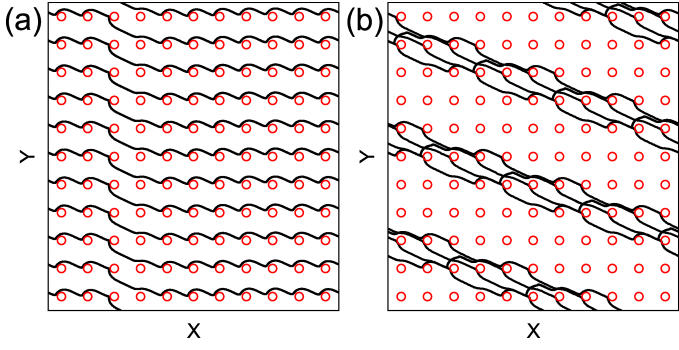


FIG. 24. Skymion trajectory (black line) and obstacle locations (red circles) for the system in Fig. 23 with  $\alpha_m/\alpha_d = 1.0$ ,  $F^D = 1.0$ , and  $x$  direction ac driving. (a) At  $A = 0.2$ , the skymion moves  $10a$  in the  $x$  direction and  $a$  in the  $y$  direction during each ac cycle. (b) An  $R = 1/3$  step at  $A = 1.0$ .

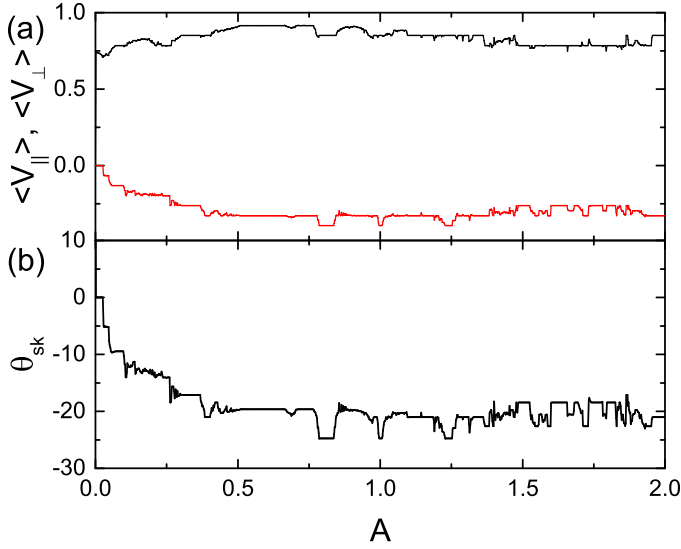


FIG. 25. (a)  $\langle V_{\parallel} \rangle$  (black) and  $\langle V_{\perp} \rangle$  (red) vs  $A$  for a system with  $\alpha_m/\alpha_d = 0.45$ ,  $F^D = 1.0$ , and  $y$  direction ac driving. (b) The corresponding  $\theta_{sk}$  vs  $F^D$ . Here the Hall angle increases in magnitude in a series of steps with increasing  $A$ .

we illustrate the trajectories for the system in Fig. 23 at  $A = 0.2$  on the  $R = 1/10$  locking step, where the skymion moves  $10a$  in the  $x$  direction and  $a$  in the  $y$  direction during each ac drive cycle. Figure 24(b) shows the same system on the  $R = 1/3$  step at  $A = 1.0$ , where the orbit jumps between two different paths to produce the  $1/3$  ratio.

In Fig. 25(a,b) we plot the velocities and  $\theta_{sk}$  versus  $A$  for the same system as in Fig. 23 but for ac driving in the  $y$ -direction. Here the Hall angle is initially zero since the skymion motion is locked along the  $x$  direction. The velocities and skymion Hall angle increase and decrease in a series of jumps as  $A$  is varied. In Fig. 26(a) we illustrate the trajectories at  $A = 0.34$  along a step on which the skymion moves  $11a$  in  $x$  and  $4a$  in  $y$  during every ac cycle. At  $A = 1.0$  in Fig. 24(b), there is a more

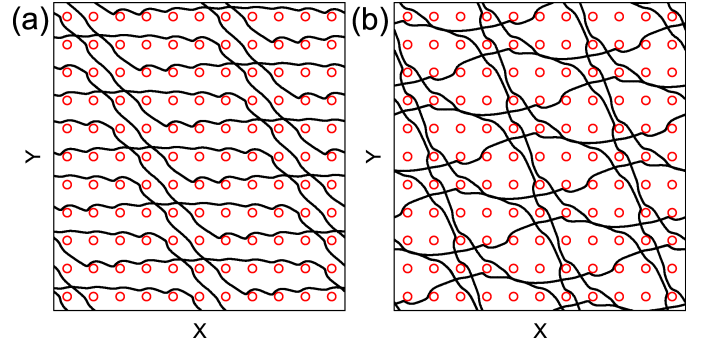


FIG. 26. Skymion trajectory (black line) and obstacle locations (red circles) for the system in Fig. 25 with  $\alpha_m/\alpha_d = 0.45$ ,  $F^D = 1.0$ , and  $y$  direction ac driving. (a)  $A = 0.34$ . (b)  $A = 1.0$ .

complicated orbit along a step where the skymion moves  $11a$  in  $x$  and  $5a$  in  $y$  per ac cycle. We find similar behavior for higher values of  $\alpha_m/\alpha_d$ . These results indicate that the Hall angle can be controlled by varying  $A$ .

## VI. DISCUSSION

In the locked phases, the skyrmions perform quantized motion along the  $x$  and/or  $y$  directions. This suggests that ac drives could be used to control skymion motion in different types of devices<sup>64</sup>. Such controlled motion could be applied to more complex geometries such as rows of pinning or different tailored geometries. We expect that similar results would appear in triangular arrays of obstacles, where the dominant directional locking angles are  $30^\circ$  and  $60^\circ$ . Future areas to address include the role of temperature, where thermal effects could strongly affect the transition points or jumps between different locking phases and could also produce thermal creep<sup>77</sup>. At higher temperatures, the phase locking effects would gradually wash away. We find that the locking effects are most prominent for systems with repulsive obstacles, but if attractive obstacles or pinning sites are used instead, the locking effects persist but are smaller for both the directional locking<sup>66</sup> and the Shapiro steps. We model the skyrmions as point particles; however, actual skyrmions often have additional internal modes of motion. These modes could be excited at much higher frequencies where they could induce additional locking frequencies. Such effects could be explored more fully with continuum based simulations<sup>78</sup>. In this work we have focused on the motion of a single isolated skymion. If multiple interacting skyrmions are present, additional locking effects could arise as a result of emergent soliton dynamics, which would be most pronounced just outside of rational filling fractions of  $1/2$  or  $1/1$ <sup>79,80</sup>, where the filling fraction indicates the ratio of the number of skyrmions to the number of obstacles or pinning sites. At commensurate fillings, the skymion-skyrmion inter-

actions should cancel and the dynamics should be similar to the single skyrmion case.

Although our results are focused on skyrmions, similar effects could arise for particles in effectively 2D systems where gyroscopic forces can arise, including active spinners<sup>81–84</sup> or charged particles in magnetic fields moving over periodic substrates<sup>85–87</sup>.

## VII. SUMMARY

We have numerically examined a skyrmion moving over a 2D periodic array of obstacles under a dc drive with an additional ac drive applied either parallel or perpendicular to the dc driving direction. We find that the Magnus force induces new types of dynamical locking effects that are not observed for overdamped systems with 2D periodic substrates. When the ac and dc drives are parallel, the skyrmion exhibits both Shapiro steps similar to those observed in the overdamped case as well as directional locking in which the skyrmion motion locks to different symmetry directions of the substrate. The locking is associated with steps or cusps in the velocities as well as changes in the skyrmion Hall angle. Under strictly dc driving, the skyrmion Hall angle changes monotonically with drive, but when ac driving is added, the skyrmion Hall angle can both increase and decrease along the locking steps. For certain ratios of the Magnus force to the damping term, we find that even though the skyrmion Hall angle is fixed in a particular direction of motion,

Shapiro steps still appear in the velocity force curves either parallel or perpendicular to the dc drive. At high drives, the skyrmion Hall angle gradually approaches the intrinsic value and shows oscillations as a function of increasing drive. In general, cusps in the velocity force curve are indicative of directional locking, while steps indicate that Shapiro steps are occurring. When the ac drive is perpendicular to the dc drive, we generally find an even larger number of steps in the velocity force curves and the skyrmion Hall angle. It is also possible to observe Hall angle overshoots in which the skyrmion Hall angle locks to a value that is much larger than the intrinsic value. When the dc drive amplitude is fixed, steps in the Skyrmion Hall angle can occur as function of changing ac drive amplitude. For higher Magnus forces, we generally find that the steps are reduced and there are increased regions of disordered flow.

## ACKNOWLEDGMENTS

This work was supported by the US Department of Energy through the Los Alamos National Laboratory. Los Alamos National Laboratory is operated by Triad National Security, LLC, for the National Nuclear Security Administration of the U. S. Department of Energy (Contract No. 892333218NCA000001). N.P.V. acknowledges funding from Fundação de Amparo à Pesquisa do Estado de São Paulo - FAPESP (Grant 2018/13198-7).

- 
- <sup>1</sup> A. Pikovsky, M. Rosenblum, and J. Kurths, *Synchronization: A Universal Concept in Nonlinear Sciences*, 1 (Cambridge University Press, Cambridge, 2001).
  - <sup>2</sup> E. Ott, *Chaos in Dynamical Systems*, 2 (Cambridge University Press, Cambridge, 1993).
  - <sup>3</sup> M. Bennett, M. F. Schatz, H. Rockwood, and K. Wiesenfeld, “Huygens’s clocks,” *Proc. Roy. Soc. A* **458**, 563–579 (2002).
  - <sup>4</sup> L. Glass, “Synchronization and rhythmic processes in physiology,” *Nature (London)* **410**, 277–284 (2001).
  - <sup>5</sup> S. Shapiro, “Josephson currents in superconducting tunneling: The effect of microwaves and other observations,” *Phys. Rev. Lett.* **11**, 80–82 (1963).
  - <sup>6</sup> A. Barone and G. Paterno, *Physics and Applications of the Josephson effect*, 6 (Wiley, New York, 1982).
  - <sup>7</sup> S. P. Benz, M. S. Rzchowski, M. Tinkham, and C. J. Lobb, “Fractional giant Shapiro steps and spatially correlated phase motion in 2D Josephson arrays,” *Phys. Rev. Lett.* **64**, 693–696 (1990).
  - <sup>8</sup> S. N. Coppersmith and P. B. Littlewood, “Interference phenomena and mode locking in the model of deformable sliding charge-density waves,” *Phys. Rev. Lett.* **57**, 1927–1930 (1986).
  - <sup>9</sup> G. Grüner, “The dynamics of charge-density waves,” *Rev. Mod. Phys.* **60**, 1129–1181 (1988).
  - <sup>10</sup> P. Martinoli, O. Daldini, C. Leemann, and E. Stocker, “ac quantum interference in superconducting films with periodically modulated thickness,” *Sol. St. Commun.* **17**, 205–209 (1975).
  - <sup>11</sup> P. Martinoli, “Static and dynamic interaction of superconducting vortices with a periodic pinning potential,” *Phys. Rev. B* **17**, 1175–1194 (1978).
  - <sup>12</sup> O. V. Dobrovolskiy, “AC quantum interference effects in nanopatterned Nb microstrips,” *J. Supercond. Novel Mag.* **28**, 469–473 (2015).
  - <sup>13</sup> L. Van Look, E. Rosseel, M. J. Van Bael, K. Temst, V. V. Moshchalkov, and Y. Bruynseraede, “Shapiro steps in a superconducting film with an antidot lattice,” *Phys. Rev. B* **60**, R6998–R7000 (1999).
  - <sup>14</sup> C. Reichhardt, R. T. Scalettar, G. T. Zimányi, and N. Grønbech-Jensen, “Phase-locking of vortex lattices interacting with periodic pinning,” *Phys. Rev. B* **61**, R11914–R11917 (2000).
  - <sup>15</sup> I. Sokolović, P. Mali, J. Odavić, S. Radošević, S. Yu. Medvedeva, A. E. Botha, Yu. M. Shukrinov, and J. Tekić, “Devil’s staircase and the absence of chaos in the dc- and ac-driven overdamped Frenkel-Kontorova model,” *Phys. Rev. E* **96**, 022210 (2017).
  - <sup>16</sup> J. Tekić and Z. Ivić, “Frequency dependence of the subharmonic Shapiro steps,” *Phys. Rev. E* **83**, 056604 (2011).
  - <sup>17</sup> M. P. N. Juniper, A. V. Straube, R. Besseling, D. G. A. L. Aarts, and R. P. A. Dullens, “Microscopic dynamics of synchronization in driven colloids,” *Nature Commun.* **6**, 7187 (2015).

- <sup>18</sup> T. Brazda, C. July, and C. Bechinger, “Experimental observation of Shapiro-steps in colloidal monolayers driven across time-dependent substrate potentials,” *Soft Matter* **13**, 4024–4028 (2017).
- <sup>19</sup> J. L. Abbott, V. A. Straube, D. G. A. L. Aarts, and R. P. A. Dullens, “Transport of a colloidal particle driven across a temporally oscillating optical potential energy landscape,” *New J. Phys.* **21**, 083027 (2019).
- <sup>20</sup> C. Reichhardt, A. B. Kolton, D. Domínguez, and N. Grønbech-Jensen, “Phase-locking of driven vortex lattices with transverse ac force and periodic pinning,” *Phys. Rev. B* **64**, 134508 (2001).
- <sup>21</sup> V. I. Marconi, A. B. Kolton, D. Domínguez, and N. Grønbech-Jensen, “Transverse phase locking in fully frustrated Josephson junction arrays: A different type of fractional giant steps,” *Phys. Rev. B* **68**, 104521 (2003).
- <sup>22</sup> C. Reichhardt, C. J. Olson Reichhardt, and M. B. Hastings, “Rectification and phase locking for particles on symmetric two-dimensional periodic substrates,” *Phys. Rev. Lett.* **89**, 024101 (2002).
- <sup>23</sup> C. Reichhardt and C. J. Olson Reichhardt, “Absolute transverse mobility and ratchet effect on periodic two-dimensional symmetric substrates,” *Phys. Rev. E* **68**, 046102 (2003).
- <sup>24</sup> J. Tekić, A. E. Botha, P. Mali, and Yu. M. Shukrinov, “Inertial effects in the dc+ac driven underdamped Frenkel-Kontorova model: Subharmonic steps, chaos, and hysteresis,” *Phys. Rev. E* **99**, 022206 (2019).
- <sup>25</sup> S. Mühlbauer, B. Binz, F. Jonietz, C. Pfleiderer, A. Rosch, A. Neubauer, R. Georgii, and P. Böni, “Skyrmion lattice in a chiral magnet,” *Science* **323**, 915–919 (2009).
- <sup>26</sup> X. Z. Yu, Y. Onose, N. Kanazawa, J. H. Park, J. H. Han, Y. Matsui, N. Nagaosa, and Y. Tokura, “Real-space observation of a two-dimensional skyrmion crystal,” *Nature (London)* **465**, 901–904 (2010).
- <sup>27</sup> N. Nagaosa and Y. Tokura, “Topological properties and dynamics of magnetic skyrmions,” *Nature Nanotechnol.* **8**, 899–911 (2013).
- <sup>28</sup> W. Jiang, G. Chen, K. Liu, J. Zang, S. G. E. te Velthuis, and A. Hoffmann, “Skyrmions in magnetic multilayers,” *Phys. Rep.* **704**, 1–49 (2017).
- <sup>29</sup> T. Schulz, R. Ritz, A. Bauer, M. Halder, M. Wagner, C. Franz, C. Pfleiderer, K. Everschor, M. Garst, and A. Rosch, “Emergent electrodynamics of skyrmions in a chiral magnet,” *Nature Phys.* **8**, 301–304 (2012).
- <sup>30</sup> J. Iwasaki, M. Mochizuki, and N. Nagaosa, “Universal current-velocity relation of skyrmion motion in chiral magnets,” *Nature Commun.* **4**, 1463 (2013).
- <sup>31</sup> S.-Z. Lin, C. Reichhardt, C. D. Batista, and A. Saxena, “Particle model for skyrmions in metallic chiral magnets: Dynamics, pinning, and creep,” *Phys. Rev. B* **87**, 214419 (2013).
- <sup>32</sup> D. Liang, J. P. DeGrave, M. J. Stolt, Y. Tokura, and S. Jin, “Current-driven dynamics of skyrmions stabilized in MnSi nanowires revealed by topological Hall effect,” *Nature Commun.* **6**, 8217 (2015).
- <sup>33</sup> S. Woo, K. Litzius, B. Krüger, M.-Y. Im, L. Caretta, K. Richter, M. Mann, A. Krone, R. M. Reeve, M. Weigand, P. Agrawal, I. Limesh, M.-A. Mawass, P. Fischer, M. Kläui, and G. S. D. Beach, “Observation of room-temperature magnetic skyrmions and their current-driven dynamics in ultrathin metallic ferromagnets,” *Nature Mater.* **15**, 501 (2016).
- <sup>34</sup> S. A. Montoya, R. Tolley, I. Gilbert, S.-G. Je, M.-Y. Im, and E. E. Fullerton, “Spin-orbit torque induced dipole skyrmion motion at room temperature,” *Phys. Rev. B* **98**, 104432 (2018).
- <sup>35</sup> J. Iwasaki, M. Mochizuki, and N. Nagaosa, “Current-induced skyrmion dynamics in constricted geometries,” *Nature Nanotechnol.* **8**, 742–747 (2013).
- <sup>36</sup> C. Reichhardt, D. Ray, and C. J. Olson Reichhardt, “Quantized transport for a skyrmion moving on a two-dimensional periodic substrate,” *Phys. Rev. B* **91**, 104426 (2015).
- <sup>37</sup> C. Reichhardt, D. Ray, and C. J. Olson Reichhardt, “Collective transport properties of driven skyrmions with random disorder,” *Phys. Rev. Lett.* **114**, 217202 (2015).
- <sup>38</sup> C. Reichhardt and C. J. O. Reichhardt, “Nonlinear transport, dynamic ordering, and clustering for driven skyrmions on random pinning,” *Phys. Rev. B* **99**, 104418 (2019).
- <sup>39</sup> W. Jiang, X. Zhang, G. Yu, W. Zhang, X. Wang, M. B. Jungfleisch, J. E. Pearson, X. Cheng, O. Heinonen, K. L. Wang, Y. Zhou, A. Hoffmann, and S. G. E. te Velthuis, “Direct observation of the skyrmion Hall effect,” *Nature Phys.* **13**, 162–169 (2017).
- <sup>40</sup> K. Litzius, I. Limesh, B. Krüger, P. Bassirian, L. Caretta, K. Richter, F. Büttner, K. Sato, O. A. Tretiakov, J. Förster, R. M. Reeve, M. Weigand, L. Bykova, H. Stoll, G. Schütz, G. S. D. Beach, and M. Kläui, “Skyrmion Hall effect revealed by direct time-resolved X-ray microscopy,” *Nature Phys.* **13**, 170–175 (2017).
- <sup>41</sup> Y.-H. Liu and Y.-Q. Li, “A mechanism to pin skyrmions in chiral magnets,” *J. Phys.: Condens. Matter* **25**, 076005 (2013).
- <sup>42</sup> J. Müller and A. Rosch, “Capturing of a magnetic skyrmion with a hole,” *Phys. Rev. B* **91**, 054410 (2015).
- <sup>43</sup> F. Büttner, C. Moutafis, M. Schneider, B. Krüger, C. M. Günther, J. Geilhufe, C. von Kor Schmising, J. Mohanty, B. Pfau, S. Schaffert, A. Bisig, M. Foerster, T. Schulz, C. A. F. Vaz, J. H. Franken, H. J. M. Swagten, M. Kläui, and S. Eisebitt, “Dynamics and inertia of skyrmionic spin structures,” *Nature Phys.* **11**, 225–228 (2015).
- <sup>44</sup> J. C. Martinez and M. B. A. Jalil, “Topological dynamics and current-induced motion in a skyrmion lattice,” *New J. Phys.* **18**, 033008 (2016).
- <sup>45</sup> C. Navau, N. Del-Valle, and A. Sanchez, “Analytical trajectories of skyrmions in confined geometries: Skyrmionic racetracks and nano-oscillators,” *Phys. Rev. B* **94**, 184104 (2016).
- <sup>46</sup> X. Gong, H. Y. Yuan, and X. R. Wang, “Current-driven skyrmion motion in granular films,” *Phys. Rev. B* **101**, 064421 (2020).
- <sup>47</sup> W. Legrand, D. Maccariello, N. Reyren, K. Garcia, C. Moutafis, C. Moreau-Luchaire, S. Coffin, K. Bouzehouane, V. Cros, and A. Fert, “Room-temperature current-induced generation and motion of sub-100 nm skyrmions,” *Nano Lett.* **17**, 2703–2712 (2017).
- <sup>48</sup> J.-V. Kim and M.-W. Yoo, “Current-driven skyrmion dynamics in disordered films,” *Appl. Phys. Lett.* **110**, 132404 (2017).
- <sup>49</sup> S. Woo, K. M. Song, X. Zhang, Y. Zhou, M. Ezawa, X. Liu, S. Finizio, J. Raabe, N. J. Lee, S. Kim, S.-Y. Park, Y. Kim, J.-Y. Kim, D. Lee, O. Lee, J. W. Choi, B.-C. Min, H. C. Koo, and J. Chang, “Current-driven dynamics and inhibition of the skyrmion Hall effect of ferrimagnetic skyrmions in GdFeCo films,” *Nature Commun.* **9**, 959 (2018).

- <sup>50</sup> R. Juge, S.-G. Je, D. de Souza Chaves, L. D. Buda-Prejbeanu, J. Peña Garcia, J. Nath, I. M. Miron, K. G. Rana, L. Aballe, M. Foerster, F. Genuzio, T. O. Montes, A. Locatelli, F. Maccherozzi, S. S. Dhesi, M. Belmeguenai, Y. Roussigné, S. Auffret, S. Pizzini, G. Gaudin, J. Vogel, and O. Boulle, “Current-driven skyrmion dynamics and drive-dependent skyrmion Hall effect in an ultrathin film,” *Phys. Rev. Applied* **12**, 044007 (2019).
- <sup>51</sup> K. Zeissler, S. Finizio, C. Barton, A. J. Huxtable, J. Massey, J. Raabe, A. V. Sadovnikov, S. A. Nikitov, R. Brearton, T. Hesjedal, G. van der Laan, M. C. Rosamond, E. H. Linfield, G. Burnell, and C. H. Marrows, “Diameter-independent skyrmion Hall angle observed in chiral magnetic multilayers,” *Nature Commun.* **11**, 428 (2020).
- <sup>52</sup> K. Litzius, J. Leliaert, P. Bassirian, D. Rodrigues, S. Kromin, I. Lemesh, J. Zazvorka, K.-J. Lee, J. Mulkers, N. Kerber, D. Heinze, N. Keil, R. M. Reeve, M. Weigand, B. Van Waeyenberge, G. Schütz, K. Everschor-Sitte, G. S. D. Beach, and M. Kläui, “The role of temperature and drive current in skyrmion dynamics,” *Nature Electron.* **3**, 30–36 (2020).
- <sup>53</sup> J. Feilhauer, S. Saha, J. Tobik, M. Zelent, L. J. Heyderman, and M. Mruczkiewicz, “Controlled motion of skyrmions in a magnetic antidot lattice,” (2019), arXiv:1910.07388.
- <sup>54</sup> D. Stosic, T. B. Ludermir, and M. V. Milošević, “Pinning of magnetic skyrmions in a monolayer Co film on Pt(111): Theoretical characterization and exemplified utilization,” *Phys. Rev. B* **96**, 214403 (2017).
- <sup>55</sup> I. L. Fernandes, J. Bouaziz, S. Blügel, and S. Lounis, “Universality of defect-skyrmion interaction profiles,” *Nature Commun.* **9**, 4395 (2018).
- <sup>56</sup> D. Toscano, S. A. Leonel, P. Z. Coura, and F. Sato, “Building traps for skyrmions by the incorporation of magnetic defects into nanomagnets: Pinning and scattering traps by magnetic properties engineering,” *J. Mag. Mag. Mater.* **480**, 171–185 (2019).
- <sup>57</sup> L. Xiong, B. Zheng, M. H. Jin, and N. J. Zhou, “Collective transport properties of skyrmions on the depinning phase transition,” *Phys. Rev. B* **100**, 064426 (2019).
- <sup>58</sup> S. Saha, M. Zelent, S. Finizio, M. Mruczkiewicz, S. Tacchi, A. K. Suszka, S. Wintz, N. S. Bingham, J. Raabe, M. Krawczyk, and L. J. Heyderman, “Formation of Néel type skyrmions in an antidot lattice with perpendicular magnetic anisotropy,” (2019), arXiv:1910.04515.
- <sup>59</sup> X. Palermo, N. Reyren, S. Mesoraca, A. V. Samokhvalov, S. Collin, F. Godel, A. Sander, K. Bouzehouane, J. Santamaria, V. Cros, A. I. Buzdin, and J. E. Villegas, “Tailored flux pinning in superconductor-ferromagnet multilayers with engineered magnetic domain morphology from stripes to skyrmions,” *Phys. Rev. Applied* **13**, 014043 (2020).
- <sup>60</sup> C. Reichhardt and C. J. Olson Reichhardt, “Shapiro steps for skyrmion motion on a washboard potential with longitudinal and transverse ac drives,” *Phys. Rev. B* **92**, 224432 (2015).
- <sup>61</sup> C. Reichhardt and C. J. O. Reichhardt, “Shapiro spikes and negative mobility for skyrmion motion on quasi-one-dimensional periodic substrates,” *Phys. Rev. B* **95**, 014412 (2017).
- <sup>62</sup> W. Chen, L. Liu, Y. Ji, and Y. Zheng, “Skyrmion ratchet effect driven by a biharmonic force,” *Phys. Rev. B* **99**, 064431 (2019).
- <sup>63</sup> W. Chen, L. Liu, and Y. Zheng, “Ultrafast ratchet dynamics of skyrmion by defect engineering under gigahertz magnetic fields,” (2020), arXiv:2002.08865.
- <sup>64</sup> A. Fert, V. Cros, and J. Sampaio, “Skyrmions on the track,” *Nature Nanotechnol.* **8**, 152–156 (2013).
- <sup>65</sup> C. Reichhardt, D. Ray, and C. J. Olson Reichhardt, “Magnus-induced ratchet effects for skyrmions interacting with asymmetric substrates,” *New J. Phys.* **17**, 073034 (2015).
- <sup>66</sup> N. P. Vizarim, C. Reichhardt, C. J. O. Reichhardt, and P. A. Venegas, “Skyrmion dynamics and topological sorting on periodic obstacle arrays,” (2020), arXiv:2001.08835.
- <sup>67</sup> B. L. Brown, U. C. Täuber, and M. Pleimling, “Skyrmion relaxation dynamics in the presence of quenched disorder,” *Phys. Rev. B* **100**, 024410 (2019).
- <sup>68</sup> C. Reichhardt and F. Nori, “Phase locking, devil’s staircases, Farey trees, and Arnold tongues in driven vortex lattices with periodic pinning,” *Phys. Rev. Lett.* **82**, 414–417 (1999).
- <sup>69</sup> C. Reichhardt and C. J. Olson Reichhardt, “Structural transitions and dynamical regimes for directional locking of vortices and colloids driven over periodic substrates,” *J. Phys.: Condens. Matter* **24**, 225702 (2012).
- <sup>70</sup> P. T. Korda, M. B. Taylor, and D. G. Grier, “Kinetically locked-in colloidal transport in an array of optical tweezers,” *Phys. Rev. Lett.* **89**, 128301 (2002).
- <sup>71</sup> M. P. MacDonald, G. C. Spalding, and K. Dholakia, “Microfluidic sorting in an optical lattice,” *Nature (London)* **426**, 421–424 (2003).
- <sup>72</sup> A. M. Lacasta, J. M. Sancho, A. H. Romero, and K. Lindenberg, “Sorting on periodic surfaces,” *Phys. Rev. Lett.* **94**, 160601 (2005).
- <sup>73</sup> D. Speer, R. Eichhorn, and P. Reimann, “Directing Brownian motion on a periodic surface,” *Phys. Rev. Lett.* **102**, 124101 (2009).
- <sup>74</sup> M. Balvin, E. Sohn, T. Iracki, G. Drazer, and J. Frechette, “Directional locking and the role of irreversible interactions in deterministic hydrodynamics separations in microfluidic devices,” *Phys. Rev. Lett.* **103**, 078301 (2009).
- <sup>75</sup> X. Cao, E. Panizon, A. Vanossi, N. Manini, and C. Bechinger, “Orientational and directional locking of colloidal clusters driven across periodic surfaces,” *Nature Phys.* **15**, 776 (2019).
- <sup>76</sup> R. L. Stoop, A. V. Straube, T. H. Johansen, and P. Tierno, “Collective directional locking of colloidal monolayers on a periodic substrate,” *Phys. Rev. Lett.* **124**, 058002 (2020).
- <sup>77</sup> C. Reichhardt and C. J. O. Reichhardt, “Thermal creep and the skyrmion Hall angle in driven skyrmion crystals,” *J. Phys.: Condens. Matter* **31**, 07LT01 (2019).
- <sup>78</sup> J. Leliaert, P. Gypens, M. Milosevic, V. B. Van Waeyenberge, and J. Mulkers, “Coupling of the skyrmion velocity to its breathing mode in periodically notched nanotracks,” *J. Phys. D* **52**, 024003 (2019).
- <sup>79</sup> C. Reichhardt and C. J. Olson Reichhardt, “Depinning and nonequilibrium dynamic phases of particle assemblies driven over random and ordered substrates: a review,” *Rep. Prog. Phys.* **80**, 026501 (2017).
- <sup>80</sup> C. Reichhardt, D. Ray, and C. J. O. Reichhardt, “Nonequilibrium phases and segregation for skyrmions on periodic pinning arrays,” *Phys. Rev. B* **98**, 134418 (2018).
- <sup>81</sup> B. C. van Zuiden, J. Paulose, W. T. M. Irvine, D. Bartolo, and V. Vitelli, “Spatiotemporal order and emergent edge currents in active spinner materials,” *Proc. Natl. Acad. Sci. (USA)* **113**, 12919–12924 (2016).



- <sup>82</sup> M. Han, J. Yan, S. Granick, and E. Luijten, “Effective temperature concept evaluated in an active colloid mixture,” *Proc. Natl. Acad. Sci. (USA)* **114**, 7513–7518 (2017).
- <sup>83</sup> C. Reichhardt and C. J. O. Reichhardt, “Reversibility, pattern formation, and edge transport in active chiral and passive disk mixtures,” *J. Chem. Phys.* **150**, 064905 (2019).
- <sup>84</sup> C. Reichhardt and C. J. O. Reichhardt, “Active microrheology, Hall effect, and jamming in chiral fluids,” *Phys. Rev. E* **100**, 012604 (2019).
- <sup>85</sup> D. Weiss, M. L. Roukes, A. Menschig, P. Grambow, K. von Klitzing, and G. Weimann, *Phys. Rev. Lett.* **66**, 2790–2793 (1991).
- <sup>86</sup> J. Wiersig and K.-H. Ahn, “Devil’s staircase in the magnetoresistance of a periodic array of scatterers,” *Phys. Rev. Lett.* **87**, 026803 (2001).
- <sup>87</sup> S. R. Power, M. R. Thomsen, A.-P. Jauho, and T. G. Pedersen, “Electron trajectories and magnetotransport in nanopatterned graphene under commensurability conditions,” *Phys. Rev. B* **96**, 075425 (2017).